

Erosive Wear Behavior of Variable Mixed-Flow Turbine Impeller Blade Under the Impact of Exhaust Particles

Taiying Wu*, Junhua Guo**, Huabing Wen***, Hongdan Liu****, Jiahao Wang* and Keliang Yu*

Keywords: Impeller blade, Exhaust particles, Erosive wear behavior, Surface roughness.

ABSTRACT

Particles in Marine diesel exhaust can cause the impeller blades to wear, thus reducing its efficiency and service life. In order to elucidate this wear mechanism, a prediction model applicable to the wear behavior of the impeller blades is developed based on the Euler-Lagrange method and the Finnie wear model. On this basis, the effects of parameters such as opening, particle size, and surface roughness on blade wear behavior and flow field after wear are analyzed. The results show that the small and large particles mainly flow through from the side of pressure surface and the tip clearance, respectively. The wear area of the impeller blade is mainly distributed in the trailing-side and rim-side of the pressure surface. The more serious the wear behavior, the greater the surface roughness, the greater the thickness of the boundary layer, and the lower the operating efficiency of the turbine. This work provides a guidance for the further design of marine diesel engines and has significant engineering implications.

INTRODUCTION

Green, environmental protection, and low carbon have become mainstream in global social development and economic growth nowadays, imposing higher requirements on emissions.

Paper Received August, 2023. Revised May, 2024. Accepted April, 2024. Author for Correspondence: Junhua Guo

* Graduate Student, School of Energy and Power, Jiangsu University of Science and Technology, Zhenjiang 212100, China.

** Instructor, School of Energy and Power, Jiangsu University of Science and Technology, Zhenjiang 212100, China.

*** Professor, School of Energy and Power, Jiangsu University of Science and Technology, Zhenjiang 212100, China.

**** Engineer, Chongqing Jiangjin Shipbuilding Industry Co. Ltd, Chongqing 402260, China.

The turbocharger is an important component of a marine diesel engine, which can raise the average intake pressure into the engine and increase the intake volume, thereby improving the efficiency of ships' diesel engines, so turbocharging technology is widely employed (Huang et al., 2020; Feneley et al., 2016; Gao et al., 2022). The turbocharger is a crucial component of a marine diesel engine. It increases the intake pressure and volume, improving the efficiency and reducing fuel consumption. However, fixed-section turbochargers have a slow response. Variable mixed-flow turbochargers are being researched as a solution to this problem and are gaining popularity in the power field (Wang et al., 2021).

Many disassembly and diagnostic tests have shown that the impeller blade surface will experience wear phenomenon due to the impact of solid particles in the exhaust gas, resulting in an increase in blade surface roughness and a decrease in operating efficiency. Marine transportation accounts for more than 90% of the global trade transportation and high oil consumption (Ahad et al., 2021), so ensuring the operational efficiency of marine diesel engines has a significant engineering and economic value.

Some important literature on structural wear behavior due to the impact of particles is listed below. Shanov and Tabakoff (1996) studied the corrosion behavior of particles on coated metals and to analyze the effects of particle impact angle, particle mass, and particle velocity on the wear rate. Hamed et al. (2005) showed that both the erosion rate and surface roughness improved with the increase in particle impact angle and particle size. Evstifeev et al. (2018) considered the effect of different flow rates and particle sizes on particle erosion, evaluated the erosion resistance of blade materials, and fitted the relationship between critical particle velocity and particle size. Panakarajupally et al. (2021) showed that the erosion rate rises with the increase in particle velocity, particle size, and temperature. Cai et al. (2015) found that boride coatings should be used as wear-resistant coatings for solid particle corrosion problems on turbine blades. Lin et al. (2018) found that the effect of

particle shape on the erosion rate was greater than that of particle size. Azimian and Bart (2016) studied particle wear from turbine combustion and analyzed the effects of rotor speed, input mass flow rate, and particle size. Xiao et al. (2017) studied the erosion of thermal barrier coatings by solid particles in a gas turbine through numerical simulations and found that turbine outlet pressure, coating thickness, and rotor speed were the key parameters affecting the reliability of the coating. Gao et al. (2022) used a CFD-DPM computational model to consider the effects of fluid-particle interactions and turbulence on particle trajectories, and also investigated the maximum erosion location and erosion rate of the turbine blades for different particle sizes, particle concentrations, and particle shape factors. Biglarian et al. (2019) numerically analyzed the wear location of the impeller at high temperature and pressure based on the Finnie model and found that the wear rate at the root of the impeller was high and in good agreement with the experiment, while showing that the Finnie model has good agreement in predicting the wear region of compressors with similar operating conditions. Finnie (1960) experimentally investigated the wear mechanism of rigid particles impacting on plastics and gave mathematical expressions for the wear rate versus particle impact velocity and angle. Wang et al., (2023) revealed the correlation between particle volume concentration, leakage vortex at the impeller top clearance and surface wear patterns of over-flow components in a semi-open impeller centrifugal pump under solid-liquid two-phase flow conditions based on the Eulerian-Lagrangian method and the Finnie wear model.

Through the review of the above literature, it can be found that (i) few scholars have studied the impact wear behavior of marine exhaust particles on impeller blades in turbines, which restricts the further optimization design of marine diesel engines; (ii) there is not yet a reasonable prediction model applicable to the characterization of the wear behavior of impeller blades impacted by marine exhaust particles. Therefore, this work intends to take the impeller blades in the variable mixed-flow turbocharger as the research object and develop a reasonable prediction model to study the wear behavior of the blades after being impacted by the exhaust particles, so as to provide design guidance for the further optimization of marine diesel engines.

The organization of this work is listed below. In Section 2, an erosive wear model for exhaust particles is developed. In Section 3, geometric and finite element models of variable mixed-flow turbine are built, and some corresponding boundary conditions are given. In Section 4, the effects of opening and surface roughness on the wear behavior and related flow field performance of impeller blades are discussed. Finally, some key conclusions are given in Section 5.

Development of erosive wear model for exhaust particles

Basic assumptions for particles

The particle size of marine diesel engine emissions ranges from several nanometers to several micrometers, the particle size distribution is approximately log-normal, and the particle modes include nucleation, accumulation, and coarse grains (Zhang et al., 2021; Feneley et al., 2016; Gao et al., 2022). In the first two modes, the particle size is generally less than 1 μm , so the particles in this work are mainly coarse particles (1-10 μm), which are composed of carbonaceous particles and mineral ash (Moldanoy et al., 2009; Ushakov et al., 2013; Francesco and Claudia, 2015; Zhou, 2019).

The exhaust gas produced during the operation of marine diesel engines contains fewer particles and the volume fraction of particles is much lower than 10%, which is a dilute phase flow. In this paper, the Euler-Lagrange method is proposed to simulate the particle operation (Sulaiman et al., 2019; Liu 2020). On this basis, the following assumptions are introduced (Kasbaoui et al., 2019, Li et al., 2023):

(i) Due to the low content of solid particles, the effect of particles on the flow field can be neglected, and the single-phase coupling method is used.

(ii) Ignoring the rotation, agglomeration, breakup and collision between the particles.

(iii) The particles are treated as spherical particles, and the geometry change of the wall surface due to particle impact is not considered, i.e., the working condition is set as a steady-state simulation.

Motion equation and wear model for particles

(i) Motion equation

The motion equation for the particle can be expressed as (Hamed et al., 2005):

$$\frac{dv_p}{dt} = \frac{18\mu C_D \text{Re}}{\rho_p d_p^2} (v_f - v_p) + \frac{g(\rho_p - \rho_f)}{\rho_p} + F_x \quad (1)$$

where, v_p and v_f are the velocities of particle and gas respectively; ρ_p and ρ_f are the density of particle and gas, respectively; g is the acceleration of gravity. The first term of the right equation in Eq. (1) is the drag force per unit mass of particle; the second term in Eq. (1) is the difference between gravity and buoyancy force per unit mass of the particle; F_x is the sum of other forces on the particle, including Saffman lift, Brownian force, and other additional forces.

(ii) Wear model

The erosion mechanism of solid particles on the wall is very complex, which is mainly reflected in two aspects: (1) erosion rate is related to the impact velocity, angle and physical properties of particles; (2) The erosion rate is related to the stiffness, ductility and roughness of the wall material.

In this work, the Finnie model (Finnie, 1960) is chosen to study the erosive wear behavior of particles

on the blade, which reflects the relationship between the impact velocity and angle of the particles and the erosion rate of the blade surface with the following expressions:

$$E = kv_p^2 f(\gamma) \quad (2)$$

Where E is the dimensionless mass; k is a constant; v_p is the particle impact velocity; γ is the impact angle and $f(\gamma)$ is a dimensionless function of the impact angle, which can be expressed as:

$$f(\gamma) = \begin{cases} \frac{1}{3} \cos^2 \gamma, & \left(\tan \gamma > \frac{1}{3} \right) \\ \sin(2\gamma) - 3 \sin^2 \gamma, & \left(\tan \gamma \leq \frac{1}{3} \right) \end{cases} \quad (3)$$

Then, the wear amount can be calculated as:

$$m_e = EN_p m_p \quad (4)$$

where m_p is the particle mass flow rate; N_p is the number of particles that hit the wall surface.

Surface roughness model

Surface roughness refers to surface unevenness due to machining or other factors. In this paper, for the treatment of surface roughness of nozzle ring and impeller blade, CFX software, wall function method, and equivalent sand roughness model are proposed to be used.

The logarithmic relationship for the near wall velocity is as follows:

$$u^+ = \frac{u_t}{u_\tau} = \frac{1}{\kappa} \ln(y^+) + C \quad (5)$$

where

$$y^+ = \frac{\rho \Delta y u_\tau}{\mu} \quad (6)$$

$$u_\tau = \sqrt{\frac{\tau_w}{\rho}} \quad (7)$$

where u^+ is the near-wall velocity; u_τ is the friction velocity; U_τ is the known tangential velocity at the distance Δy from the wall; y^+ is the dimensionless distance from the wall; τ_w is the wall shear stress; κ is the Von Karman constant; C is the logarithmic layer constant, depending on the wall roughness; ρ is the density.

The roughness of the wall surface can significantly increase the degree of near-wall turbulence and can in turn cause an increase in the heat transfer coefficient and shear stress at the wall surface. Therefore, in order to make the effect of surface roughness coincide better with the experimental results, the effect of roughness is considered in CFX software using the following relation:

$$u^+ = \frac{U_i}{u_\tau} = \frac{1}{\kappa} \ln(y^+) + B - \Delta B \quad (8)$$

where $B = 5.2$ and the offset ΔB can be expressed as:

$$\Delta B = \frac{1}{\kappa} \ln(1 + 0.3\tilde{k}_s) \quad (9)$$

Where the relationship between the equivalent sand grain roughness k_s and the modified sand grain roughness \tilde{k}_s can be written as:

$$\tilde{k}_s = \frac{k_s \bar{u}_\tau}{\nu} \quad (10)$$

where ν is the fluid kinematic viscosity.

In addition, the relationship between the equivalent sand roughness k_s and the geometric mean roughness R_a can be expressed as (Mirko et al., 2011; Koch and Smith, 1976):

$$k_s = 6.2R_a \quad (11)$$

NUMERICAL SIMULATION SETTINGS

Geometric and finite element models of variable mixed-flow turbine

In this work, the turbine end of variable mixed-flow turbocharger (see Figure 1(a)) is numerically analyzed. The geometric model is shown in Figure 1(b), including the inlet tract, volute, impeller, and blades of nozzle ring (named b1 to b24 according to the clockwise direction), and its main geometric parameters are listed in Table 1. The variable turbine opening range is 0%, 25%, 50%, 75%, and 100%, where 0% opening represents the case of the smallest nozzle ring throat area, i.e. the shortest distance between the throats, and 100% opening represents the case when the nozzle ring is at the maximum throat area. Opening increases with the diesel engine operating load, matching the engine under different operating conditions.

For the inlet tract and volute of the turbine, it is proposed to use a tetrahedral mesh to mesh them, due to their irregular structure and large curvature variation along the circumference; for the nozzle ring and impeller, a professional turbine blade channel meshing software Turbogrid is used to mesh them hexahedrally and encrypt the blade surface and the tip clearance, as shown in Figure 1 (c) and (d).

Generally, the more the number of meshes, the more accurate the calculation results of the model are, but the correspondingly more computational resources are required. In order to ensure the accuracy of the calculation results while avoiding the need for excessive computational resources, the meshes are verified to be irrelevant. Taking the turbine at 25% opening and 30000 r/min speed as an example, the single-channel model is simulated when the grid numbers are 1.46 million, 1.94 million, 2.4 million, and 3.05 million, respectively. The calculation results are shown in Table 2. Obviously, after the grid number reaches to 2.4 million, the calculation result of each parameter basically tends to be stable. Therefore, considering the calculation accuracy and calculation volume, the grid number of about 2.4 million for calculation is intended to choose in this work.

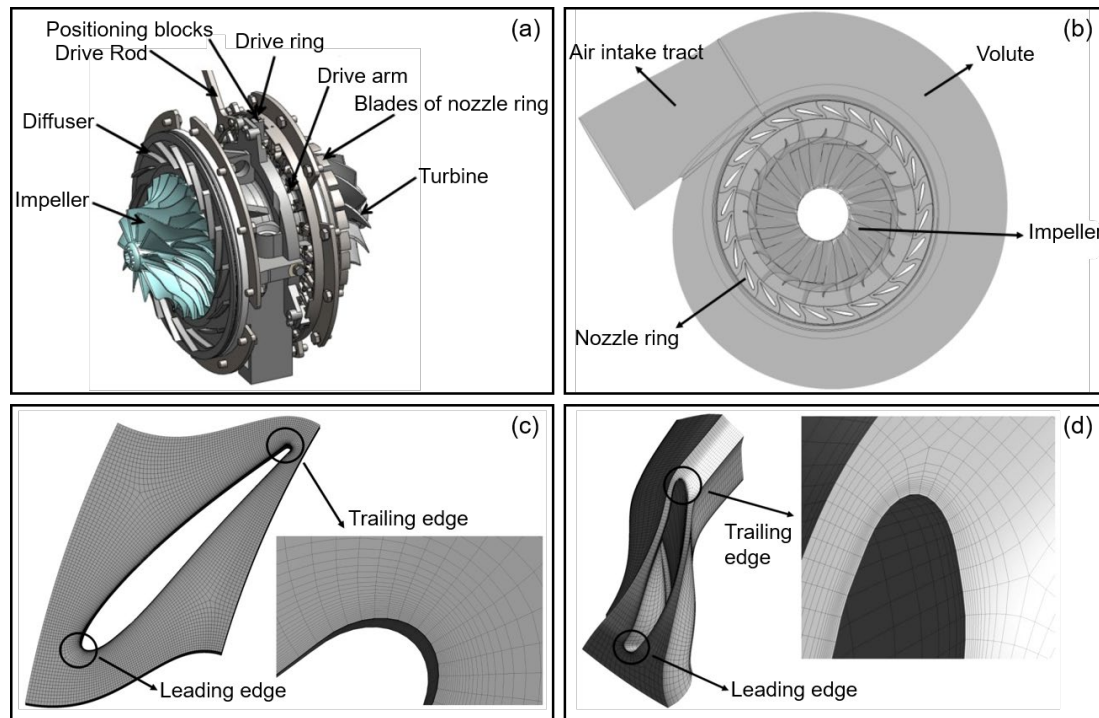


Fig. 1. (a) Schematic of variable mixed-flow turbocharger, (b) geometric model of turbine, (c) mesh model of nozzle ring, and (d) mesh model of impeller.

Table 1. Main geometrical parameters of turbine

Parameters	Value
Number of blades of nozzle ring	24
Number of impeller blades	12
Radius of air inlet (mm)	64.0
Radius of air outlet (mm)	91.0
Inlet radius of nozzle ring (mm)	132.0
Outlet radius of nozzle ring (mm)	106.0
Leaf top clearance of impeller (mm)	1.0

Table 2. Grid-independence verification

No. of grids	Efficiency	Outlet flow (kg/s)
1460000	76.58%	0.9745
1940000	75.83%	0.9669
2400000	75.62%	0.9627
3050000	75.65%	0.9631

Boundary condition settings

The working medium of the turbine is continuous high-speed compressible air, which contains exhaust gases and particulate matter from fuel combustion, and the flow field inside it is typical of turbulent flow. Therefore, in this work, the Reynolds-averaged Navier-Stokes equations and the SST turbulence model are used, where the turbulent shear stress is considered by the SST model, which is suitable for flow simulations containing inverse pressure gradients(Smirnov and Menter, 2005).

On the basis of the above model, the following

boundary conditions are set according to the actual working conditions of the turbocharger:

(i) Continuous phase: turbine inlet is set to total temperature and pressure, outlet is set to atmospheric pressure, airflow inlet direction is vertical turbine inlet interface, turbulence intensity is defined as the ratio of turbulent pulsation velocity to mean velocity. All solid wall surfaces are smooth and adiabatic, with no-slip velocity boundary. At the intersection of the stationary and rotating regions inside the turbine, the frozen rotor boundary condition is used, and the mixed intersection is used for the other intersections.

(ii) Particle phase: At the turbine inlet, the slip velocity of the particles is zero, i.e. the incident velocity of the particles is the same as the inlet velocity of the airflow, and the particles enter perpendicular to the turbine inlet with random position. The particles are soot particles produced by the combustion of marine diesel engines; therefore, the density is set to 2000 kg/m³, the diameter distribution range is set to 1~10 μm, the inlet mass flow rate is set to 1×10⁻³ g/kg, and the number is set to 5000. It should be noted that 5000 is not the actual number of particles, but only the degree of refinement of their spatial distribution.

Surface roughness settings

During actual operation, the percentage of turbine running time under different openings within a certain phase is not fixed, but varies with the actual situation. Referring to the weighting coefficients used for the test cycle of the constant-speed marine main engine in the specification "Guidelines for Testing and Investigating the Emission of Nitrogen Oxides from Marine Diesel

Engines (2011 Edition)", the percentage of turbine at different openings is set as shown in Table 3.

In order to analyze and compare the effect of different surface roughness on the turbine operation under different openings, the turbine operation time is set as 1000h, 2000h, 3000h, 4000h and 5000h, and the surface roughness under different operation time is calculated by the wear rate of nozzle ring and impeller blade obtained from the numerical simulation of ANSYS, and the surface roughness is calculated differently due to the wear of each nozzle ring and each impeller blade, so the average is taken to set the geometrically averaged roughness R_a , as shown in Table 4.

Table 3. Running time distribution of different turbine openings

Opening	100%	75%	50%	25%	0%
Weighting factor	0.2	0.3	0.3	0.1	0.1

Table 4. Surface roughness at different running times

Running time (h)	1000	2000	3000	4000	5000
R_a (μm)	51	103	154	205	257

RESULTS AND DISCUSSIONS

Verification of the prediction model

Based on the particle erosion wear test on 90° bends in the literature (Chen 2004), the same geometrical model of the bends is established, and the numerical simulation of particle erosion wear is carried out using the Finnie wear model, and the simulation results are compared and analyzed with the experimental data in the literature.

The test setup consists of a compressor, a flow meter, a test part and a pipe, simplified as shown in Fig.2(a). The test part, shown in Fig.2(b), is a 90° bend with a diameter of the bend $D = 25.4 \text{ mm}$ and a radius of the bent section $r = 38.1 \text{ mm}$. The measurement position of wear is shown in the bent pipe section marked by the circle in Fig.2(c), α is the angle of the bend ($0\sim 90^\circ$), and 7 measurement points are selected at 10° intervals in the measurement position of wear.

In the experiment, a profilometer is used to measure the surface profile before and after the erosion test at the same location to determine the local thickness loss, the experiment is carried out three times, and the experimental results are averaged, in order to ensure the stability of the flow field calculation in the process of numerical solution and to facilitate the convergence, respectively, the inlet and outlet sections of the bend are extended, and the extension length is $L=76.2\text{mm}$, and the geometrical model of the bend is shown in Fig.2(d).

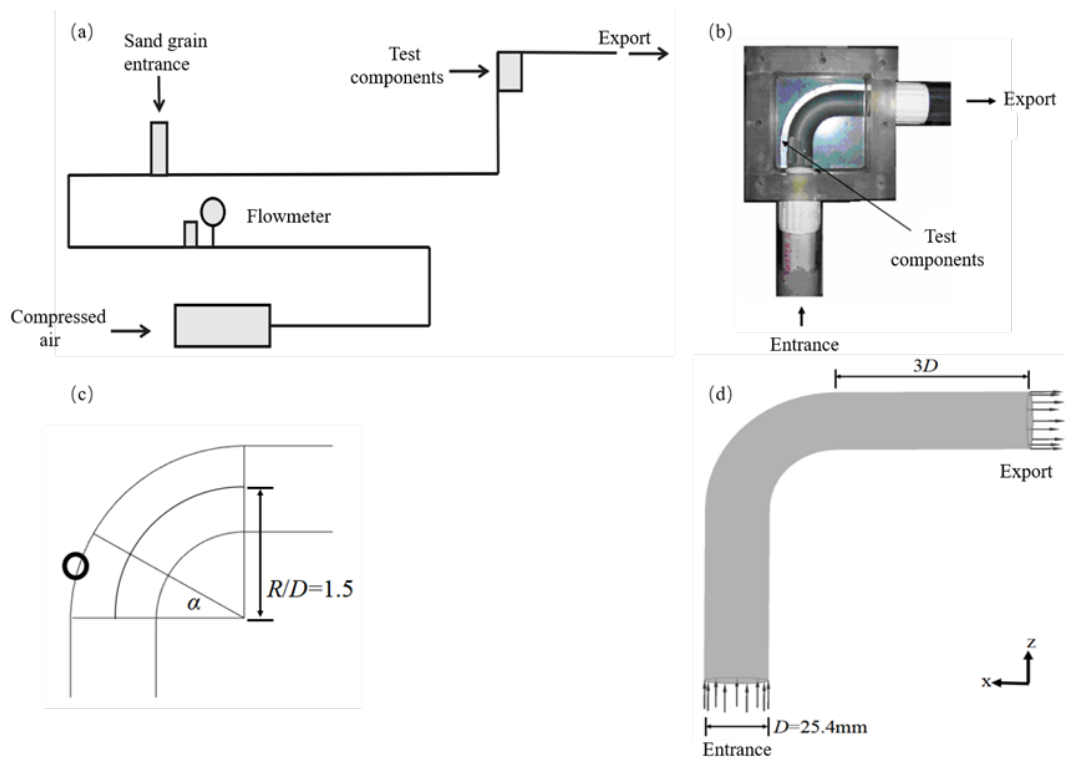


Fig.2. Experimental diagram of test and simulation: (a) Simplified diagram of experimental apparatus; (b) Test components ;(c) Measurement positions ; (d) Geometric model of elbow.

As can be seen in Fig.3, the overall agreement between the numerical simulation results and the experimental results is high, indicating the accuracy of the calculated results of the adopted wear model.

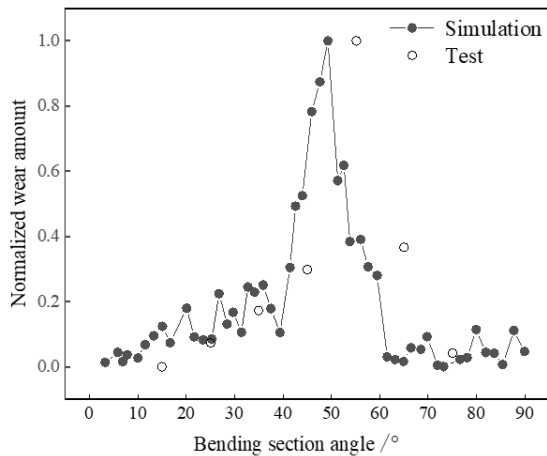


Fig.3. Comparison of simulated and experimental normalized erosion.

Effect of opening on the flow field of impeller blades

Figure 4 shows the Mach number distribution and streamline diagram of impeller blades at 50% blade height under different openings.

From Fig.4 (a1, b1, and c1), it can be seen that as the opening increases, the airflow undergoes expansion and acceleration in the impeller channel. When the air enters the impeller and is squeezed by its pressure surface, a vortex separation zone is formed at the suction front edge, and a low-speed zone is formed at the pressure front edge. With the increase of the opening, the low-speed zone decreases gradually and shifts to the leading-edge of the blade, and the vortex separation zone decreases gradually until it disappears. The reason is that, with the increase of the opening, the angle between the trailing-edge of the nozzle ring and the leading-edge of the blade gradually decreases, making the positive inlet air attack angle is reduced, the airflow distribution is more uniform, and the airflow streamline is closer to the blade surface.

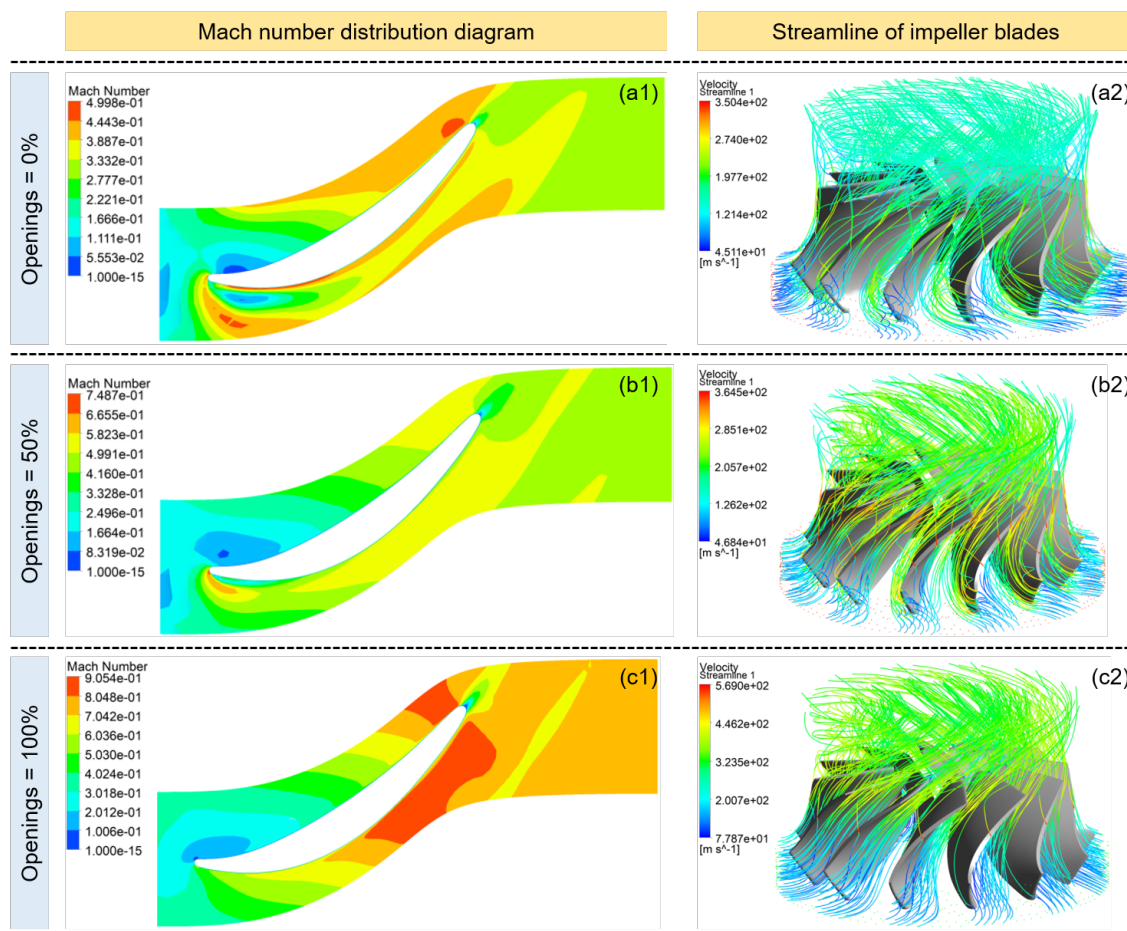


Fig.4. Mach number distribution and streamline diagram of impeller blades at 50% blade height under different openings.

It can be seen from Fig.4 (a2, b2, and c2) that when the opening is small, part of the airflow needs to bypass the leading-edge of the blade to reach the side

of suction surface. With the increase of the opening, this phenomenon is relieved. In fact, this is also the reason why the airflow forms a vortex separation zone

at the edge of the suction surface. The presence of low-speed zone and vortex separation zone at the leading-edge of the blade increases the flow loss, and the separation and deceleration of the airflow can also be observed at the trailing-edge of the blade, which is more obvious with the increase of opening.

In addition, the existence of the tip clearance between the impeller and the turbine cover makes some of the airflow flow from the pressure surface side to the leaf tip and mix with the airflow on the suction

surface side, thus resulting in increased flow loss. However, as the opening increases, the airflow in the impeller is more uniformly distributed, and the airflow through the gap at the top of the blades is reduced, and the airflow increases steeply in speed when passing through because the gap space is small. Besides, the airflow from the tip clearance carries some particles, which can cause wear on the rim side of the impeller blade.

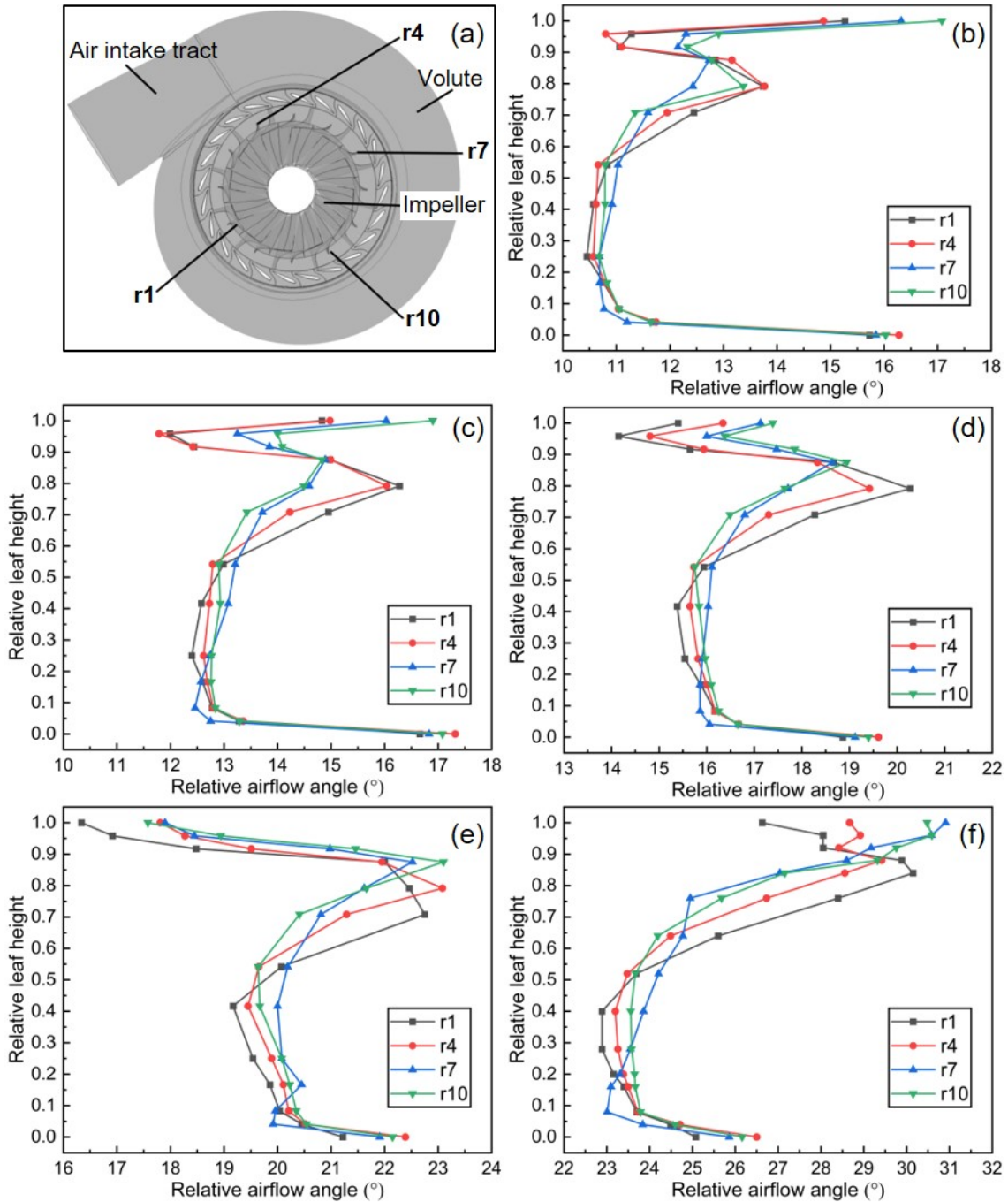


Fig.5. Comparison of inlet relative airflow angle distribution of impeller blades along the blade height under different openings: (a) naming schematic of impeller blades, (b) 0% opening, (c) 25% opening, (d) 50% opening, (e) 75% opening, and (f) 100% opening.

Effect of opening on the inlet relative airflow angle of impeller blades

The circumferential asymmetry of the inlet volute structure of the turbine causes the distribution of the flow field inside the turbine to vary along the circumference, leading to variations in the particle motion within each blade impeller, and consequently in the wear of the impeller blades at different positions. As shown in Figure 5(a), the impeller blades are named as r1 ~ r12 in clockwise order, and considering the large number of impeller blades, only four impeller blades (r1, r4, r7, and r10) are selected as representatives for analysis in this paper. The four selected impeller blades divide the turbine along the inlet direction of the airflow, representing the overall pattern.

Comparing Figure 5(b)~(f), it can be seen that under different openings, the distribution of the inlet relative airflow angle of the impeller blade at different positions along the blade height varies, and the difference of the airflow angle in the upper part of the blade height is greater than that in the lower part, especially in the area where the relative blade height is 0.6 ~ 0.8. This phenomenon suggests varying airflow movement within different locations of the impeller blades, correspondingly causing a difference in the movement of the particles, and thus leading to the wear area and wear amount of each impeller blade is also

different.

Effect of opening on the erosive wear behavior of impeller blades

Figure 6 and Figure 7 show the wear rate distributions of the pressure and suction surfaces of the impeller blades under different openings, respectively. Among them, the blades are sorted in the way shown in Figure 6(a), and the marked 'max' and 'min' indicate the impeller blades with the largest and smallest average wear rates, respectively.

From Fig.6, it can be seen that, on the whole, the wear area and wear amount of the pressure surface of the impeller blade are increasing with the increase of opening. Under different openings, the wear situation of each blade at the same position of each pressure surface is similar, i.e., the wear rate and wear area do not have significant differences, which indicates that the motion trajectory of the particles in the flow channel on the pressure surface side of each blade under different openings is similar. Specifically, the wear area of the blade pressure surface occurs mainly in the rear half of the blade and on the rim-side, with more severe wear near the rim-side. However, almost no wear occurs on the leading-edge side of the blade, and only at 100% opening, a weak degree of wear can be observed on the leading-edge side of some blades.

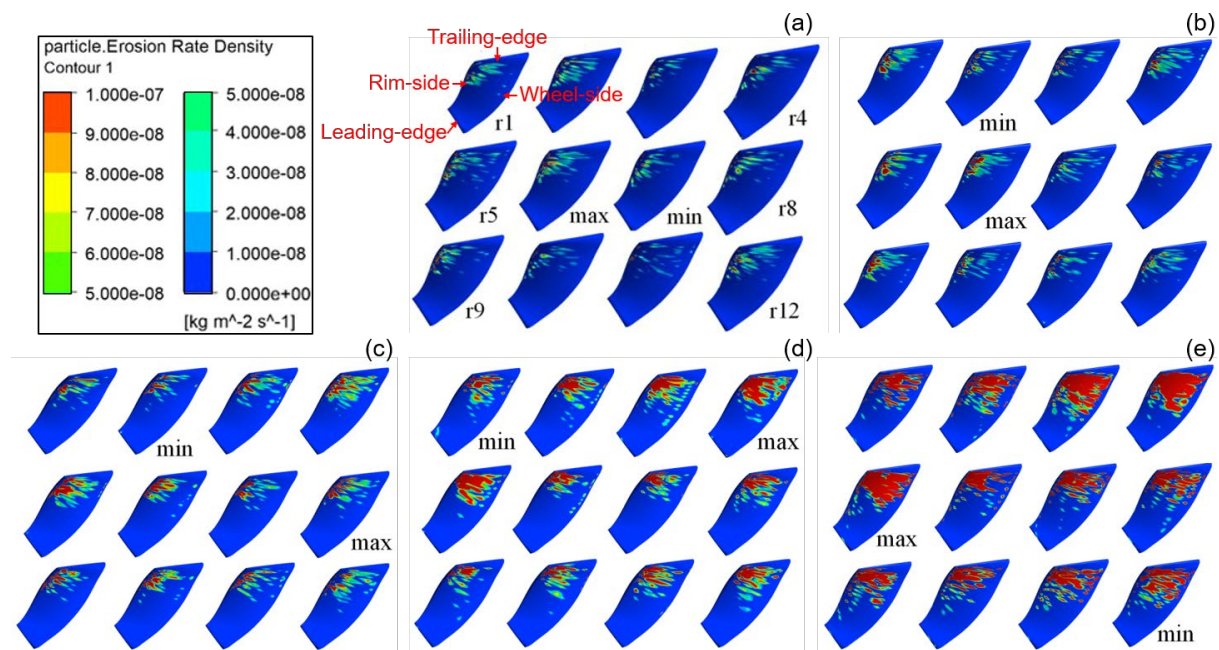


Fig.6. Distribution clouds of the wear rate on pressure surface of impeller blade under different openings: (a) 0% opening, (b) 25% opening, (c) 50% opening, (d) 75% opening, and (e) 100% opening.

It can be found from Fig.7 that the blade suction surface is little affected by the erosive wear of the particles, only at 0% and 25% the opening, some of the blades are subjected to the erosive wear by the particles, and the wear behavior only occurs in a small

part of the area at the leading-edge of the suction surface. When the opening is above 50%, almost no wear occurs on the suction surface, indicating that the particles have stopped hitting the suction surface at these situations. Compared with the pressure surface of

the blade, the wear amount and wear area of the suction surface are significantly smaller than the pressure surface, indicating that the airflow is biased towards

the pressure surface of the blade, thereby causing the particles mainly to hit the pressure surface (Huang et al., 2019).

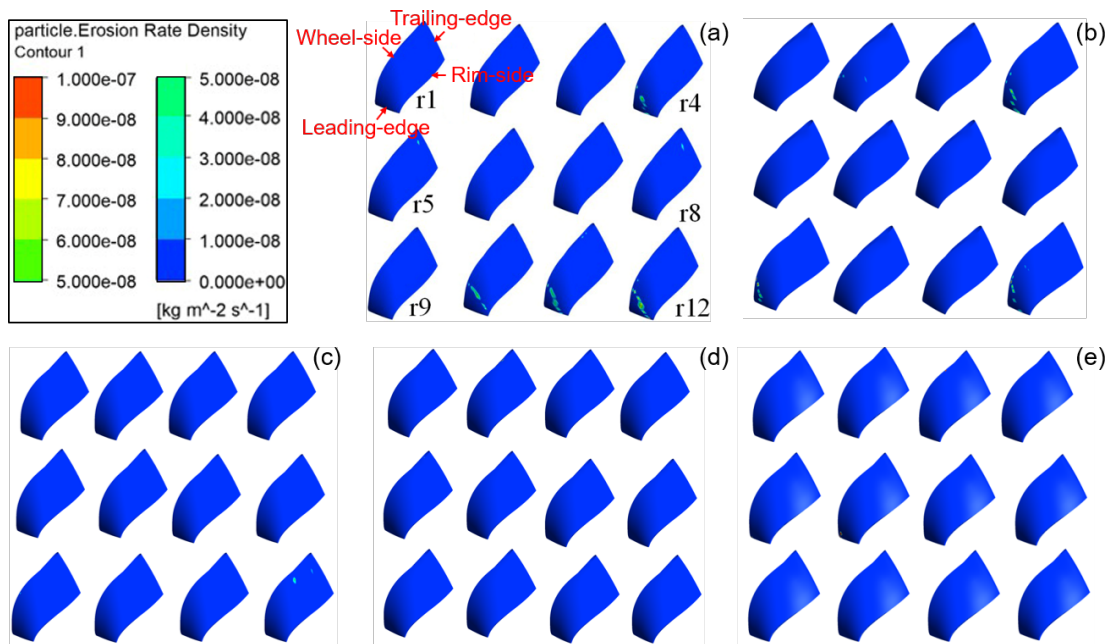


Fig.7. Distribution clouds of the wear rate on suction surface of impeller blade under different openings: (a) 0% opening, (b) 25% opening, (c) 50% opening, (d) 75% opening, and (e) 100% opening

Figure 8(a) shows the comparison of the average wear rate of each impeller blade under different openings. When the opening is 0%, 25%, and 50%, the wear amount of the same blade has little difference, all in the range of $(3.9\sim 52.3)\times 10^{-9}$ $\text{kg}/(\text{m}^2\times\text{s})$, and the wear amount between different blades is also similar. When the opening reaches 75%, the wear amount of the blade increases significantly, and the gap in wear amount between different blades also increases. Lastly, when the opening reaches 100%, the wear amount increases sharply, and the value range can reach $(98.6\sim 864)\times 10^{-$

$\text{kg}/(\text{m}^2\times\text{s})$, which is much higher than the values the other openings, and for the average wear rate of the impeller blade, the value under the maximum opening is as much as 33 times of the minimum opening, indicating that the influence of the opening on the wear amount of the impeller blade is very significant.

Figure 8(b) shows the photograph of the actual wear of impeller blade, it can be seen that the wear degree of the pressure surface is obviously suction surface, which verifies the reasonableness of the above simulation to a certain extent.

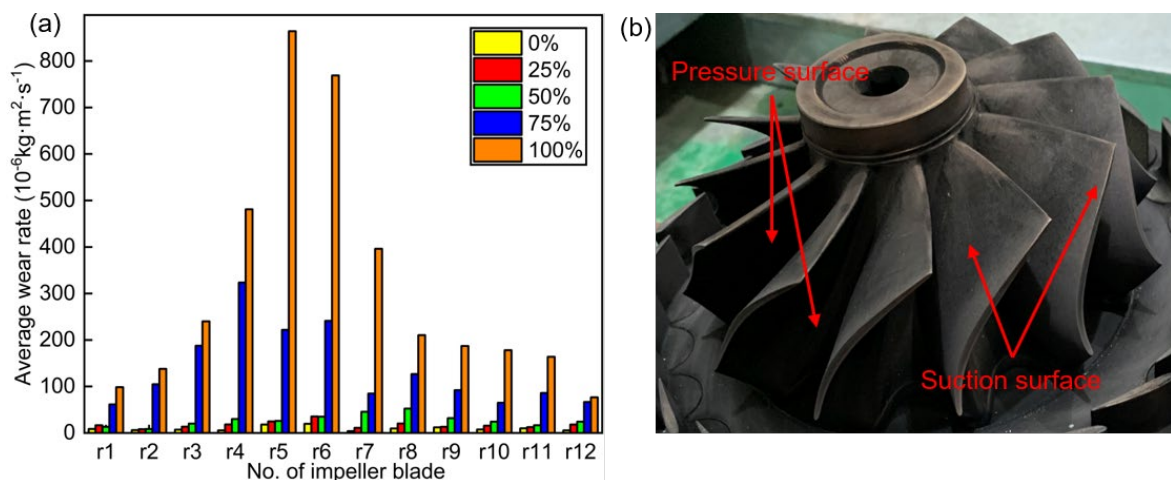


Fig.8. (a) The average wear rate of each impeller blade under different openings, (b) wear morphology of actual impeller blades.

Effect of opening and size on the particle trajectory

Figure 9 illustrates the particle trajectories with the sizes of 1 μm , 5 μm , and 10 μm in the impeller under 0%, 50%, and 100% opening. Note that the blades shown in Fig.9 are the ones with the highest average wear rate. As can be seen in Fig.9, the particle trajectories can be divided into two types: (1) particles flowing through the impeller blade runners; (2) particles flowing through the tip clearance (about 1 mm).

For the particles with 1 μm , their own inertia is

small, coupled with the large influence of the airflow, leading them to basically flow with the airflow on the side near the pressure surface of the blade under all openings, and their trajectory is more uniformly distributed along the circumferential direction. However, for particles with 5 μm and 10 μm , their relatively large mass leads to a higher centrifugal force during impeller rotation, which in turn makes them mostly pass through the tip clearance, and the distribution of particles along the circumference becomes non-uniform as the opening increases.

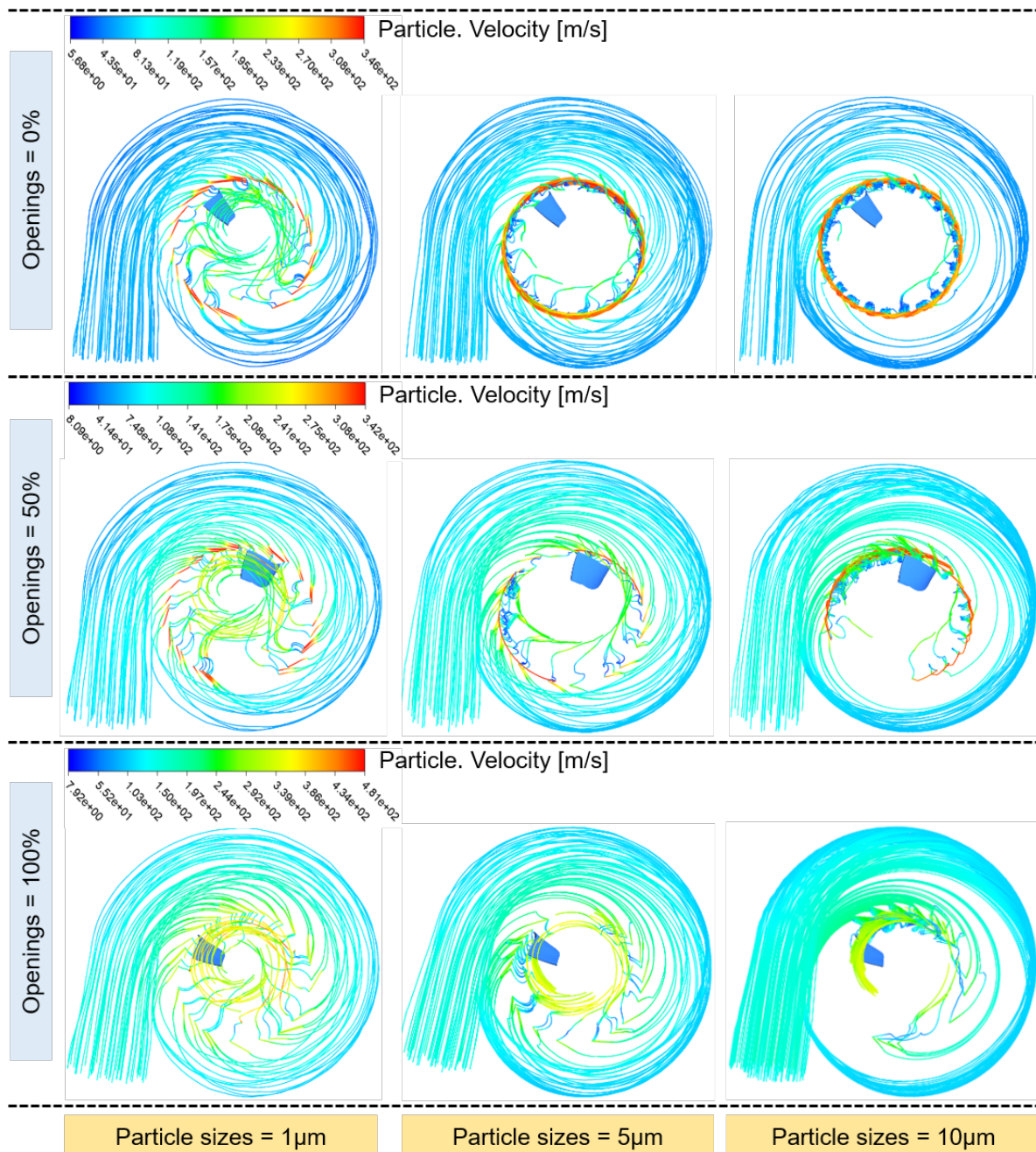


Fig.9. Trajectory of particles with different sizes in the impeller under different openings

Specifically, when the opening is small, the trajectory of the particles with 5 μm is relatively uniformly distributed along the circumferential direction, but when the opening is above 50%, the distribution of the particle trajectory along the circumferential direction begins to deviate, and the deviation increases as the opening increases, especially in the vicinity of the blade with the largest average

In summary, it can be seen that the large particles are mainly flowing from the tip clearance, resulting in the wear area of the impeller blade mainly occurs in the pressure surface of the blade on the rim-side. In addition, by the influence of the flow field distribution, the circumferential distribution of the particle trajectory is not uniform, which in turn causes the wear amount and wear area of the blade at different positions also exist differences.

Effect of surface roughness on the airflow velocity of impeller blade

Figure 10 shows the velocity distribution of impeller blade r5 (the most worn impeller blade) at 50% blade height under 0% and 100% opening when the roughness is 0 μm (smooth), 103 μm , and 251 μm .

Obviously, as the surface roughness of the impeller blade increases, the thickness of the flow boundary layer on both sides of its suction surface and pressure surface increases, and the thickness of the boundary layer on the suction surface is greater than

wear rate, where the particle trajectories are very dense. For particles with 10 μm , the distribution of particle trajectories along the circumference is already not uniform even at 0% opening, but the difference is not significant. When the opening is increased to 50%, more particles can be found clustered near the blades with the largest average wear rate. This phenomenon is more pronounced when the opening reaches to 100%. that on the pressure surface. The reason for this phenomenon is that the greater the roughness is, the greater the obstruction of airflow on the blade surface is, resulting in a thicker boundary layer. Moreover, the airflow on the suction surface side of the blade has a stretching effect, while the airflow on the pressure surface side has a squeezing effect, resulting in the boundary layer thickness on the suction surface being greater than that on the pressure surface.

When the opening is relatively small, the airflow under the action of inertia by the blade pressure surface extrusion, in the leading-edge of the suction surface formed a vortex separation zone, which decreases with the increase of surface roughness; in the leading-edge of the pressure surface exists a low-speed zone, which also decreases with the increase of surface roughness. In addition, the phenomenon of deceleration and slight separation of the airflow is observed at the trailing-edge of the blade, which becomes more obvious with the increase of surface roughness.

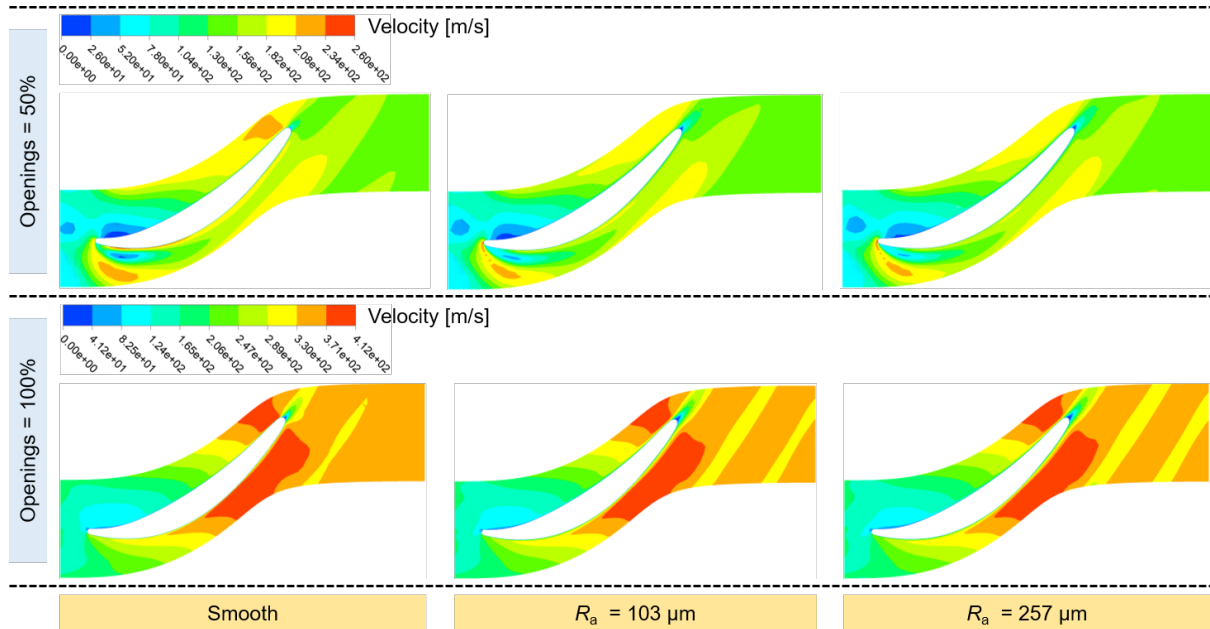


Fig.10. Effect of roughness on the velocity distribution of impeller blade r5 at 50% blade height under different openings

Effect of surface roughness on the friction coefficient of impeller blade

Figure 11 shows the distribution of surface friction coefficient of impeller blade r5 at 50% blade height for different roughness under 0%, 50%, and 100%

opening, respectively. It can be found that the surface friction coefficient increases with the increase of roughness, which leads to the increase of the thickness of the flow boundary layer, and consequently makes the increase of the flow loss.

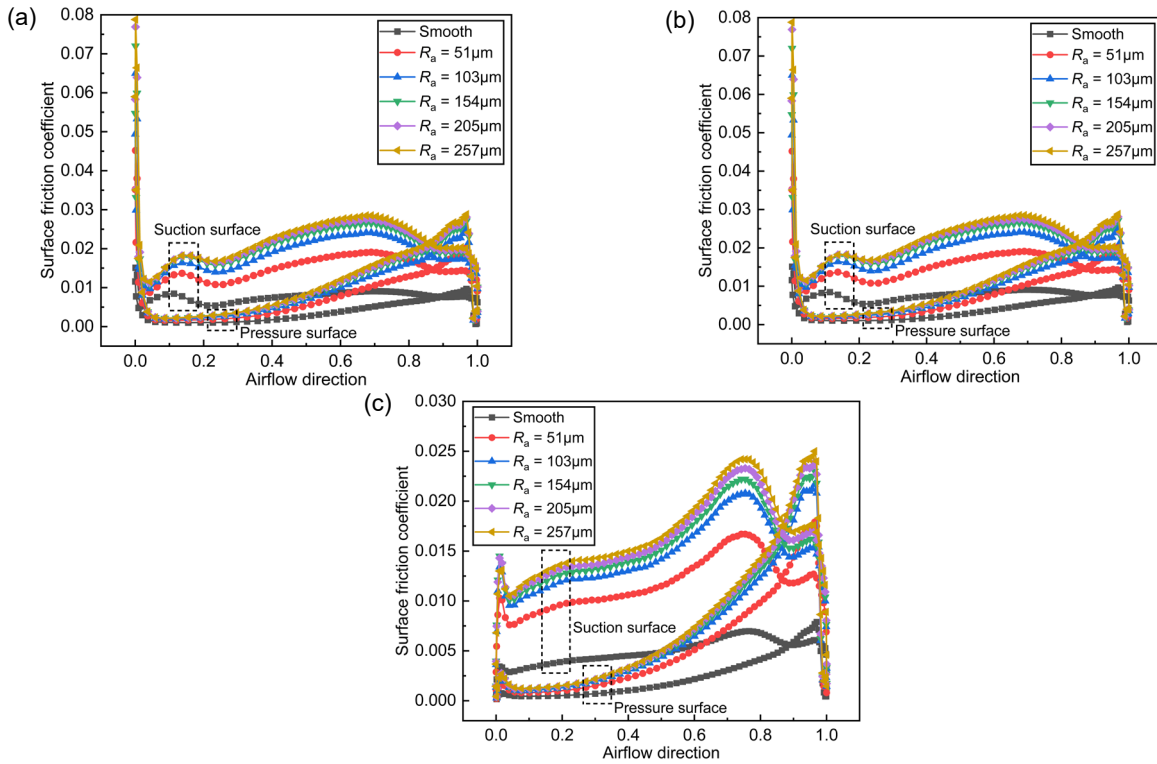


Fig.11. Effect of roughness on surface friction coefficient of impeller blade r5 at 50% blade height under different openings: (a) 0% opening, (b) 50% opening, and (c) 100% opening

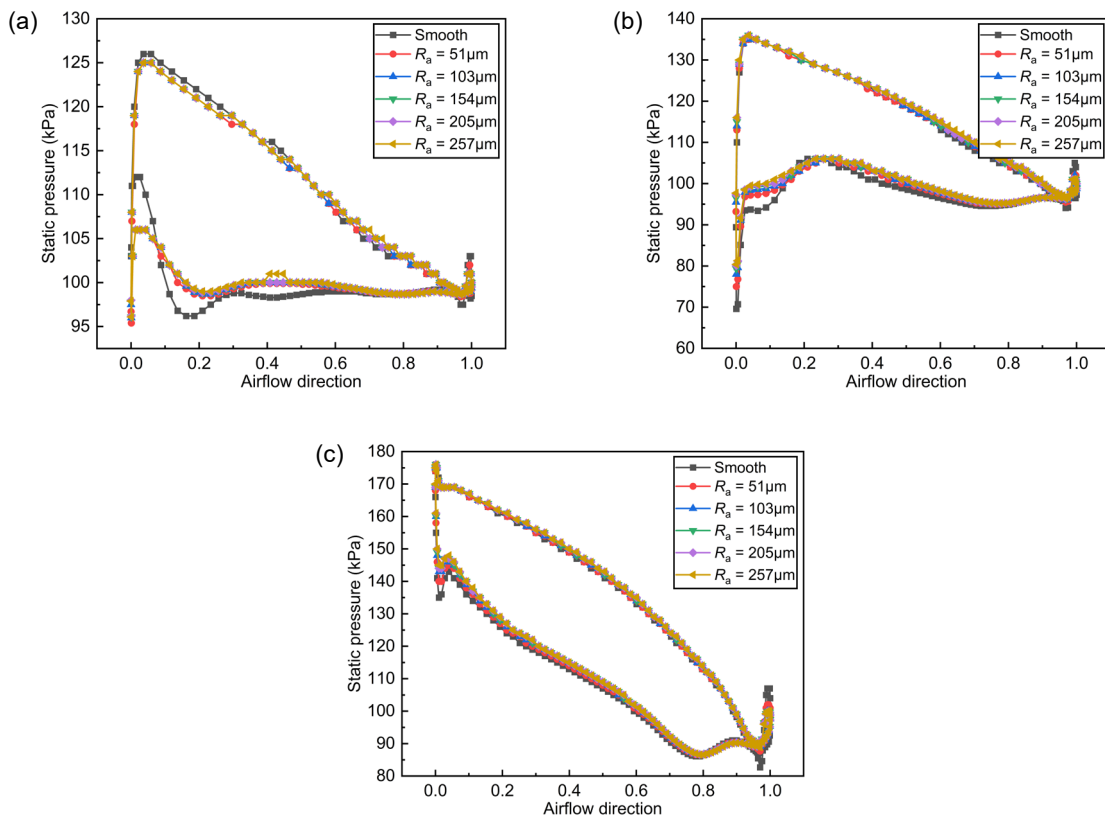


Fig.12. Effect of surface roughness on static pressure distribution of impeller blade r5 at 50% blade height under different openings: (a) 0% opening, (b) 50% opening, and (c) 100% opening

For the pressure surface, the surface friction coefficient increases gradually along the airflow direction, reaching a peak at about 0.95 in the airflow direction, and then decreases sharply. For the suction surface, there is a vortex separation zone at its leading-edge, resulting in an extreme value of the friction coefficient there, and with the increase of the opening, the vortex separation zone gradually decreases, the friction coefficient at this place also decreases, and the extreme value also shifts to the trailing-edge of the blade.

In addition, with the increase of the opening, the overall surface friction coefficient of the impeller blade decreases, which is mainly due to the more uniform airflow distribution at the impeller inlet after the increase of the opening, making the effect of roughness on airflow reduced.

Effect of surface roughness on the static pressure of impeller blade

Figure 12 shows the static pressure distribution of impeller blade r5 at 50% blade height with different roughness under 0%, 50%, and 100% opening. It can be found that under the same opening, the static pressure of the suction surface and pressure surface of the blade are increased with the increase of roughness, and the change of the static pressure of the suction surface is larger than that of the pressure surface, while the static pressure gap between these two surfaces is reduced with the increase of roughness, reducing the aerodynamic performance of the impeller blade, and thereby leading to the decrease of turbine efficiency (Base et al., 2022).

In addition, comparing the static pressure distribution of the blade under different openings, it can be found that, with the opening increases, the difference of static pressure on both sides of the blade under different roughness becomes smaller, the reason is that the opening increases, the airflow increases, and the flow rate decreases, resulting in the effect of roughness on static pressure decreases.

CONCLUSIONS

In this work, a prediction model is developed for the impeller blades subjected to erosive wear by marine exhaust particles. Subsequently, a finite element model of the flow field at the turbine end in a variable mixed-flow turbocharger is established, and the boundary conditions for numerical simulation are given. On this basis, the effects of factors such as openness and surface roughness on the erosive wear behavior of impeller blades are investigated, and some conclusions with practical engineering significance are obtained, which are listed as follows:

(i) The movement of particles varies along the circumference, due to the circumferential asymmetry of the turbine flow field distribution, which in turn leads to differences in the wear amount and wear area

of the impeller blades at different locations.

(ii) Impeller blade wear area is mainly distributed in the trailing-side and rim-side of the pressure surface, while very little wear occurs on the suction surface. With the increase of the opening, the wear amount, wear area, and wear difference between different blades are all increased.

(iii) The small particles in the impeller blade mainly flow through from the side of pressure surface, while the large particles mainly flow through the tip clearance due to the centrifugal force, and the opening has little effect on the particle flow position.

(iv) The thickness of flow boundary layer and the surface friction coefficient on both sides of the suction surface and pressure surface of impeller blade improve with an increase in surface roughness, leading to an increase in flow loss near the boundary layer, but its increase rate begins to decrease.

(v) The static pressure on suction surface and pressure surface of impeller blade increases with an increase in surface roughness, but the static pressure difference between these two surfaces decreases with the increase of the surface roughness, thus reducing the aerodynamic performance of the blade.

From the actual wear of the impeller blades and the simulation results, it can be seen that the distribution of the surface wear area leads to the distribution of the actual surface roughness is not uniform, so the surface of the blade can be subsequently divided into separate areas and set different surface roughness to study the changes in the turbine's internal flow field and aerodynamic performance.

ACKNOWLEDGMENT

This work was supported by Postgraduate Research & Practice Innovation Program of Jiangsu Province (SJCX21_1788).

References

- Ahad, A ,E., Eric, C, O., Yusuf, B., Tareq, A, A., “A review of cleaner alternative fuels for maritime transportation,” *Energy Reports.*, pp. 1962-1985 (2021).
- Azimian, M., Bart, H, J., “Computational analysis of erosion in a radial inflow steam turbine,” *Engineering Failure Analysis.*, pp. 26-43 (2016).
- Biglarian, M., Momenilarimi, M., Ganji, B., “Prediction of erosive wear locations in centrifugal compressor using CFD simulation and comparison with experimental model,” *Journal of the Brazilian Society of Mechanical Sciences and Engineering.*, pp. 106 (2019).
- Base, A., Gianfranco, S., Manh-Vu, T., “Numerical analysis on the effect of blade roughness on cavitating flow characteristics in centrifugal

- pumps,” *Journal of the Brazilian Society of Mechanical Sciences and Engineering.*, PP. 1-14 (2022).
- Cai, L, X., Mao, J, R., Wang, S, S., Di, J., Feng, Z., “Experimental investigation on erosion resistance of iron boride coatings for steam turbines at high temperatures,” *Proceedings Of The Institution Of Mechanical Engineers Part J-Journal Of Engineering Tribology.*, pp. 636-645 (2015).
- Chen, X., “Application of computational fluid dynamics (CFD) to flow simulation and erosion prediction in single-phase and multiphase flow,” Oklahoma: The University of Tulsa., pp. 1-78 (2004).
- Evstifeev, A., Kazarinov, N., Petrov, Y., Witek, L., Bednarz, A., “Experimental and theoretical analysis of solid particle erosion of a steel compressor blade based on incubation time concept,” *Engineering Failure Analysis.*, pp. 15-21 (2018).
- Feneley, A, J., Pesiridis, A., Andwari, A, M., “Variable geometry turbocharger technology for exhaust energy recovery and boosting-a review,” *Renewable and Sustainable Energy Reviews.*, pp. 959-975 (2016).
- Finnie, I., “Erosion of surfaces by solid particles,” *Wear.*, pp. 87-103 (1960).
- Francesco, D, N., Claudia, C., “Particulate matter in marine diesel engines exhausts: Emissions and control strategies,” *Transportation Research Part D: Transport and Environment.*, pp.166-191 (2015).
- Gao, J., Liu, Y., Zheng, Q., Liang, C., “Advances in aerodynamic, structural design and test technology of variable geometry turbines,” *Proceedings Of The Institution Of Mechanical Engineers Part A-Journal of Power and Energy.*, pp. 364-390 (2022).
- Gao, Y., Liu, H., Lin, Y., Gu, Y., Wang, S., “Numerical investigation of the erosion behavior in blades of tidal current turbine,” *Journal of Renewable and Sustainable Energy.*, pp. 1-18 (2022).
- Hamed, A, A., Tabakoff, W., Rivir, R, B., Das, K., Arora, P., “Turbine Blade Surface Deterioration by Erosion,” *Journal of Turbomachinery.*, pp. 445-452 (2005).
- Huang, S., Huang, J., Guo, J., Mo, Y., “Study on Wear Properties of the Flow Parts in a Centrifugal Pump Based on EDEM-Fluent Coupling,” *Processes.*, pp. 1-11 (2019).
- Huang, L., Chen, X., Li, X., Zhang, W., Wang, X., Huang, M., “Development status of marine diesel engine turbocharging technology,” *Journal of Propulsion Technology.*, pp. 2438-2449 (2020).
- Koch, C, C., Smith, L, H., “Loss sources and magnitudes in axial-flow compressors,” *Journal Of Engineering For Gas Turbines And Power.*, pp. 411-424 (1976).
- Kasbaoui, M, H., Koch, D, L., Desjardins, O., “Clustering in Euler-Euler and Euler-Lagrange simulations of unbounded homogeneous particle-laden shear,” *Journal of Fluid Mechanics.*, pp. 174-203 (2019).
- Lin, N., Arabnejad, H., Shirazi, S, A., McLaury, B, S., Lan, H., “Experimental study of particle size, shape and particle flow rate on Erosion of stainless steel,” *Powder Technology.*, pp. 70-79 (2018).
- Liu, K., “Systematic Evaluation and Improvement of Euler-Lagrange Methodology: Application to Spray Control,” University of Florida ProQuest Dissertations Publishing., pp. 28151185 (2020).
- Li, W., Shi, H., Yu, X., “A DEM-based Euler–Lagrange model for motion of particle–fluid two-phase mixtures,” *Acta Geotechnica.*, pp. 1-19 (2023).
- Mirko, M., Michele, P., Ruggero, S, P., Venturini, M., “Numerical analysis of the effects of nonuniform surface roughness on compressor stage performance,” *Journal Of Engineering For Gas Turbines And Power.*, pp. 1-8 (2011).
- Moldanov, J., Fridell, E., Popovicheva, O., Demirdjian, B., TishkovaV., Faccineto, A., Focsa, C., “Characterisation of particulate matter and gaseous emissions from a large ship diesel engine,” *Atmospheric Environment.*, pp. 2632-2641 (2009).
- Panakarajupally, R, P., Mirza, F., Rassi, J, E., Morscher, G, N., Abdi, F., Choi, S., “Solid particle erosion behavior of melt-infiltrated SiC/SiC ceramic matrix composites (CMCs) in a simulated turbine engine environment,” *Composites Part B: Engineering.*, pp.108860 (2021).
- Shanov, V., Tabakoff, W., “Erosion resistance of coatings for metal protection at elevated temperatures,” *Surface and Coatings Technology.*, pp. 88-93 (1996).
- Smirnov, P, E., Menter, F, R., “Sensitization of the SST Turbulence Model to Rotation and Curvature by Applying the Spalart-Shur Correction Term,” *Journal Of Turbomachinery.*, pp. 041010 (2009).
- Sulaiman, M., Hammouti, A., Climent, E., Wachs, A., “Coupling the fictitious domain and sharp interface methods for the simulation of convective mass transfer around reactive particles: Towards a reactive Sherwood number correlation for dilute systems,” *Chemical Engineering Science.*, pp. 334-351 (2019).
- Ushakov, E., Valland, H., Nielsen, J, B., Hennie, Erik., “Particle size distributions from heavy-duty diesel engine operated on low-sulfur marine fuel,” *Fuel Processing Technology.*, pp. 350-358 (2013).
- Wang, Z., Ma, Z., Zhu, F., “Performance of a variable geometry turbine with elastically restrained guide vanes under pulsating conditions,”

- Transactions of Beijing Institute of Technology., pp. 706-712+780 (2021).
- Wang, K., L, H., W, L., L, J., “Effects of particle volume concentration on the leakage vortex and erosion characteristics of semi-open centrifugal pumps,” Transactions of the Chinese Society of Agricultural Engineering (Transactions of the CSAE)., pp. 44-53 (2023).
- Xiao, Y., Yang, L., Zhou, Y., Wei, Y., Wang, N., “Dominant parameters affecting the reliability of TBCs on a gas turbine blade during erosion by a particle-laden hot gas stream,” *Wear.*, pp. 166-175 (2017).
- Zhang, F., Chen, Y., Su, P., Cui, M., Han, Y., Matthias, V., Wang, G., “Variations and characteristics of carbonaceous substances emitted from a heavy fuel oil ship engine under different operating loads,” *Environmental Pollution.*, pp.117388 (2021).
- Zhang, F., Guo, H., Chen, Y., Matthias, V., Zhang, Y., Yang, X., Chen, J., “Size-segregated characteristics of OC, EC and organic matters in PM emitted from different types of ships in China,” *Atmospheric Chemistry And Physics.*, pp.1549-1564 (2020).
- Zhou, J., “Research on particulate matter emission characteristics of marine diesel engine and its control technology,” Harbin Engineering University., pp.12-53 (2018).